Roberto Aguilar Ayala[1,2], Morgan A. Crabtree[2], Matthew L. Hancock[2], Alexander Jarnot[3], Janine E. Captain[2], Julie Kleinhenz[4], Erin Rezich[5], Kris Zacny[6], Vincent Vendiola[6], Zack Mank, Kenneth C. Wright[7], Jaime L. Winfield[7], Thomas Orlando[8], Brant Jones[8], Phil Metzger[9], Jaqueline W. Quinn[2]

Mass Spectrometry Monitoring of Drilling Operations in Water-Doped Lunar Simulant under Cryogenic Conditions

Abstract:

The utilization of analytical instruments for the detection and quantification of volatiles on the Moon is crucial for the development of in situ resource utilization technology. A test campaign under cryogenic conditions aimed to simulate the cold lunar environment of permanently shadowed regions (PSRs). The test campaign was performed in a Thermal Vacuum Chamber (TVAC) equipped with a bin of regolith simulant doped at three increasing water concentrations delineated at specific depths (Dry, 2.5, and 5 wt%, respectively). The average operating pressure of the chamber was 1.6×10^{-6} Torr with an average regolith temperature of -178°C. Four holes were drilled into the regolith simulant bin using The Regolith and Ice Drill for Exploring New Terrain (TRIDENT) drill. The resulting cuttings-piles and their volatile activity were monitored via the Mass Spectrometer observing lunar operations (MSolo) instrument to determine the extent to which a mass spectrometer can monitor the release of volatiles during drilling activities in lunar-like environments. The results of this campaign helped to plan for the operation and subsequent data interpretation of the Polar Resources Ice Mining Experiment-1 (PRIME-1) mission on the Moon.

[1] Corresponding author roberto.aguilar-ayala@nasa.gov
[2] NASA Kennedy Space Center, FL 32899
[3] NASA Langley Research Center, Hampton, VA 23666
[4] NASA Johnson Space Center, Houston, TX 77058
[5] NASA Glenn Research Center, Cleveland, OH 44135
[6] Honeybee Robotics, Altadena, CA 91001
[7] IMI Adaptas, Palmer, MA 01069
[8] Georgia Institute of Technology, Atlanta, GA 30332
[9] University of Central Florida, Orlando, FL 32816

Table of Figures

Introduction:

Missions to the moon including Clementine and Lunar Prospector indicate the presence of hydrogen-bearing volatiles locked within the lunar surface (Nozette *et al.*, 1996; Feldman *et al.*, 1998). However, it was not until the Lunar Crater Observation and Sensing Satellite (LCROSS) mission that the identification and measurement of several volatile species was verified in a permanently shadowed region (PSR) of the Cabeus crater: water ice was confirmed within its impact zone at approximately 5.6 ± 2.9% by mass (Colaprete *et al.*, 2010). Knowing now that a significant concentration of volatiles is trapped within the cold environments of the lunar south pole, key information such as localization of resources, the actual concentrations, and the volatile distribution based on depth are all still to be determined. A fundamental component for long-term space exploration requires the extraction and utilization of resources within the sites of exploration (Sanders and Larson, 2013). In-Situ Resource Utilization (ISRU), as the name suggests aims to develop technology to extract and use the available resources located within the surface of the Moon, thus providing a foundation for human habitation and exploration.

A clear aspiration for future ISRU missions is to fully understand the available resources on the Moon. Prospecting missions on the lunar surface that involve drilling operations along with analytical instruments for the detection and quantification of volatiles on the Moon will be crucial to understanding the volatile distribution on and below its surface. During a Thermal Vacuum Chamber (TVAC) test campaign in 2019, a drill known as TRIDENT (The Regolith and Ice Drill for Exploration of New Terrains) was coupled to a test unit of MSolo (Mass Spectrometer observing lunar operations) to monitor water ice release from regolith simulant during drilling operations in simulated lunar environments. The results of this test campaign discussed in this report show a relationship between water ice concentration and the signal detected by MSolo during the drilling operations that could be leveraged for the PRIME-1 mission in addition to future lunar missions.

1. Experimental Set Up

1.1. MSolo Mass Spectrometer

The MSolo instrument is a modified commercial off-the-shelf (COTS) mass spectrometer based on INFICON's Transpector® MPH residual gas analyzer. This mass spectrometer was ruggedized for space applications by replacing electrical components with improved, radiation-resistant components and

incorporating structural and thermal enhancements necessary for withstanding vibrations experienced during launch and in the harshness of the space environment. All modifications were implemented without changing the COTS-like operation. MSolo is capable of an operational scanning range of mass-to-charge ratios (*m/z*) 1-100. The operating mass range allows for the detection of volatile species (for this test, most notably water, hydrogen, and nitrogen), their relative intensities, and isotopic ratios. MSolo utilizes a crossbeam ion source (XB) configuration, which consists of a redundant set of linear filaments that ionize gas-phase molecules traveling perpendicular to the direction of the electron beam and generates a small current signal as an output. The geometric configuration of the crossbeam ion source design allows for a higher density of electrons to be introduced into the ionization region, thus ionizing molecules traveling axially through the anode cage without interacting with its surfaces. This configuration is exceptionally useful for the detection of released volatiles from a point source whilst minimizing background effects. Figure 1 illustrates the crossbeam configuration in relation to the two available filaments. MSolo works by introducing the generated ions into the quadrupole, where they are filtered based on their *m/z* and subsequently detected by a Faraday cup, or an electron multiplier, if higher sensitivity is required. For these tests, the instrument operated across the full scanning range, and while the dwell time for all masses was set to 32 ms, the dwell time for the water signal (*m/z* 18) was increased to 256 ms to target the release of water from drilling activities. The electron multiplier was also calibrated so that the nitrogen signal (*m/z* 28) peak (the most abundant background peak in the chamber) reached a target signal of approximately 6×10^{-8} A, thus maximizing the detectable signal of the entire mass range without saturating the detector with the background signal. The baseline signal of the instrument for this test was 3.71×10^{-13} A.

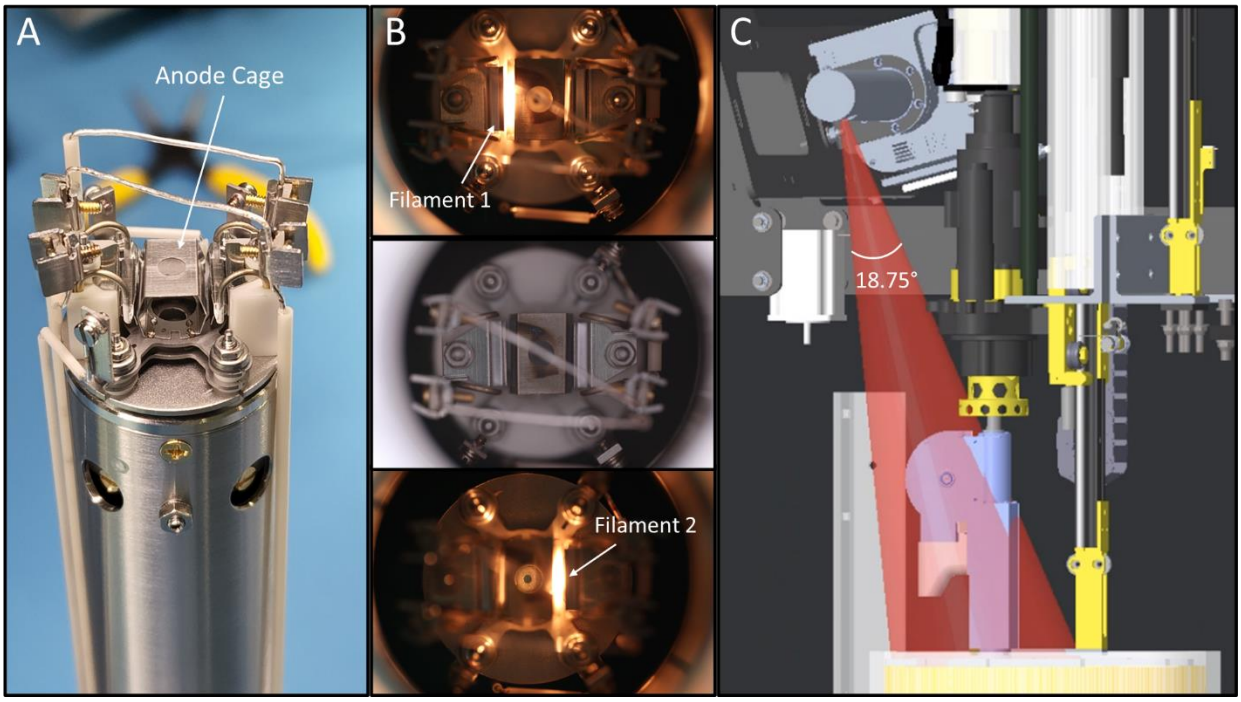

Figure 1: Cross Beam ion source configuration of MSolo (A), showing the two linear filaments (B) in correlation to the anode cage and the correlation to its field-of-view (C) used to determine optimized detection of regolith cuttings pile volatile release.

MSolo was mounted on a bracket attached to a translator frame connected to TRIDENT, allowing it to maintain a constant distance from the drill hole/pile even as the drill moved between locations. MSolo's location relative to the bracket and drill was determined based on the alignment necessary for the drill cuttings pile to be within the instrument's field of view (FOV), an 18.75-degree cone. The molecules within this FOV have a direct path from the pile surface to the detector. A visual representation of MSolo's location and FOV is shown in Figure 1C.

1.2. TRIDENT Drill

TRIDENT is a drilling system designed and built by Honeybee Robotics for the acquisition of volatile-rich samples from planetary subsurfaces. The drill was incrementally developed for over two decades and went through extensive technological development with validation tests performed in planetary analog locations such as Antarctica, Arctic, and Atacama, as well as in TVACs. TRIDENT's main features were developed from the Icebreaker-3 mission configuration and the drill was mass-optimized

during the Life in the Atacama (LITA) project (Paulsen *et al.*, 2018; Zacny *et al.*, 2023). The TRIDENT drill is shown in Figure 2.

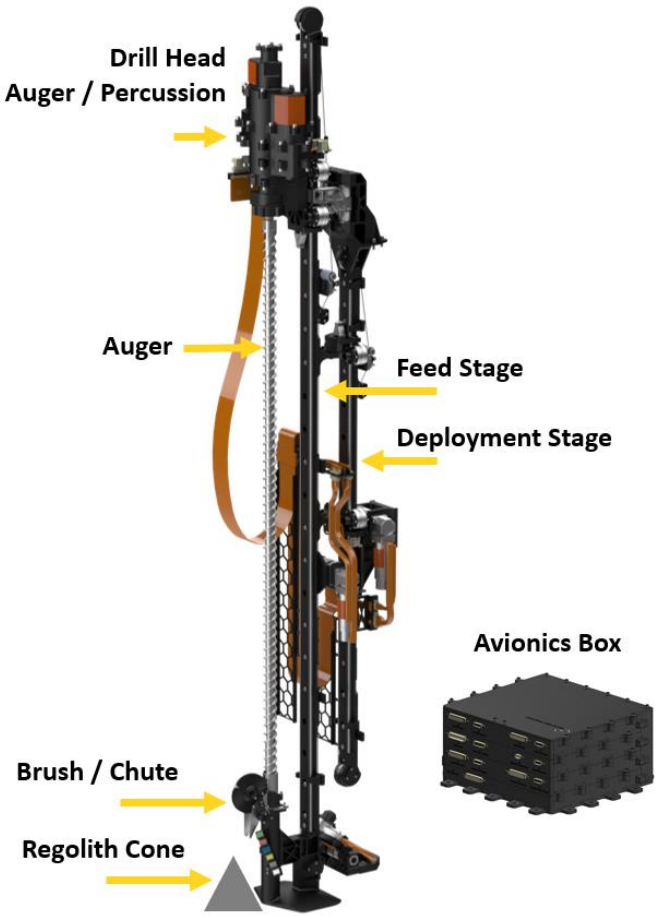

Figure 2: TRIDENT Drill

TRIDENT features a rotary-percussive drill head driven by two separate actuators. Splitting rotation and percussion allows the drill to use three modes of operation: rotation-only, percussion-only, and rotation-percussion. This flexibility helps preserve drilling energy as not all drilling operations require use of percussion. It also allows use of percussion-only operation in certain circumstances including clearing cuttings from auger flutes and seismic sensing. The drill has an 1.2 m auger with a full-faced carbide bit at its end, allowing for a full one-meter drill depth. The “bite” section is the lower 15 cm of the auger. This region has deep, low-pitched flutes, making it well-suited to cuttings capture. The upper section of the auger has shallower, high-pitched flutes that are better for cuttings conveyance. The auger

drills and captures cuttings in 10 cm bites – after 10 cm of regolith is penetrated, the auger is lifted from the resulting hole, and the captured cuttings are brushed off the auger onto the surface forming a pile via a brushing subsystem. The auger is then lowered back into the hole and the process is repeated, resulting in a conical cuttings pile that grows with each bite.

The bite sampling approach has numerous advantages. Subsurface stratigraphy is preserved in at least 10 cm sections, potentially on the order of millimeters under ideal conditions. Lifting the auger every 10 cm lowers the energy required for drilling, as at a depth of 1 m, the power required to move the total mass of cuttings from the entire hole to the surface could be significantly greater than power required to drill. Finally, pauses in drilling allow the drill bit and auger to cool off between bites, thus minimizing volatile gas impacts.

1.3. Glenn Research Center VF-13 Chamber

The VF-13 is a cylindrical chamber with an internal volume of 6.35 m^3 (Figure 3A) located at NASA's Glenn Research Center (GRC). The chamber includes a removable lid measuring 2.52 m in height and 1.5 m in diameter and a fixed base with a depth of 1.08 meters that accommodates all the electrical, mechanical, and gas feedthroughs. A removable cold wall is placed inside the lid and a cold shell clamped around the regolith bin sits in the fixed base of the chamber. The cold wall and regolith bin can be independently temperature controlled from room temperature down to approximately 90 K using liquid nitrogen, and the average operating chamber pressure for this test campaign was approximately $1.6x10^{-6}$ Torr.

All test article hardware (e.g. TRIDENT and MSolo) was mounted on a trolley rig that can be moved in two dimensions using remotely-actuated stepper motors and chain drives, allowing access to the entire surface of the regolith bin (Figure 3B). As such, multiple drill holes were drilled without needing to break vacuum to replace the regolith sample or change location. The MSolo instrument was integrated into the trolley system using a custom bracket, permitting the instrument and drill to move simultaneously and to maintain a constant distance (19.32 cm) from the plane of the regolith with a high degree of rotational freedom.

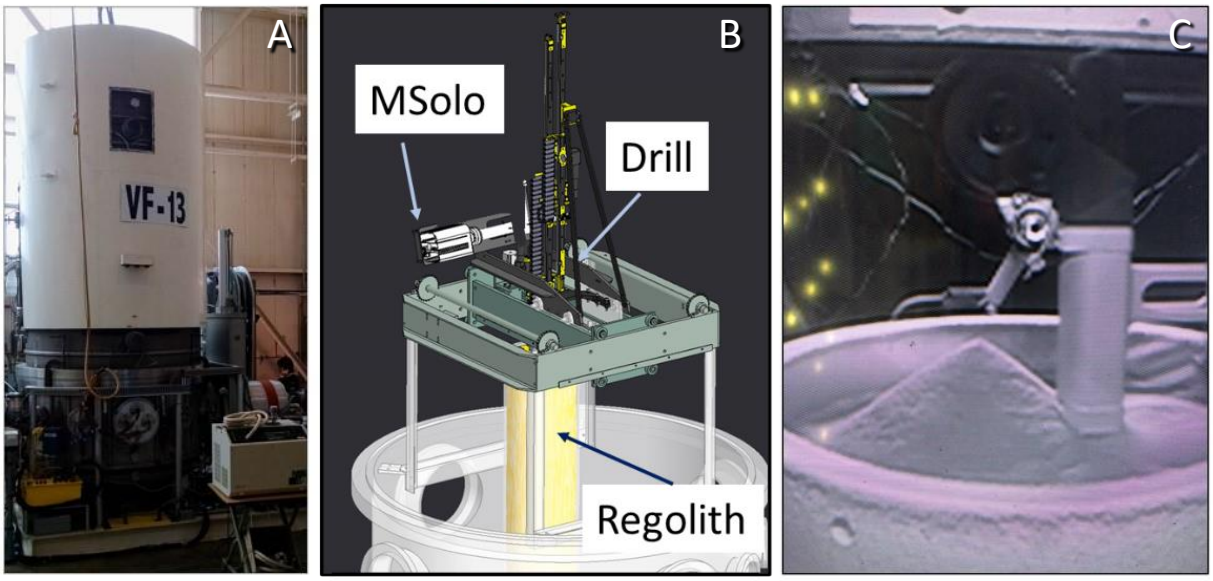

Figure 3: Experimental set up in VF13 chamber: closed VF13 chamber (A), CAD drawing of experimental set up showing MSolo's location relative to the drill and regolith bin (B), cuttings cone (C).

Regolith simulant sample was contained within a 1.2 m tall cylindrical aluminum bin with an inner diameter of 0.278 m. The bin accommodates up to four drill holes (4B). Soil temperatures were recorded via three ports at various heights along the regolith bin equipped with three to five type-T thermocouples embedded in the regolith at different radial positions.

1.4. Test Conditions

After the vacuum chamber was pumped down and cooled, the TRIDENT drill took multiple bites from a single drill hole while the MSolo instrument scanned continuously to detect volatile species being emitted from the regolith pile. This bite approach was repeated in four trolley positions so that four drill holes were analyzed within the regolith bin (Figure 4B).

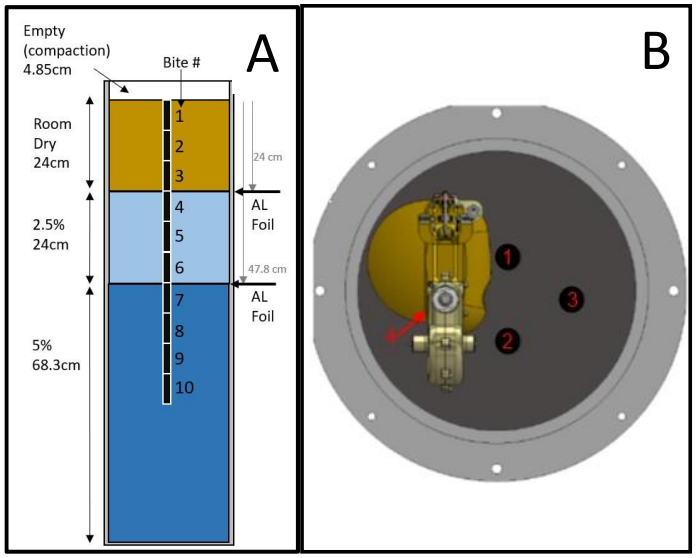

Figure 4: Regolith bin testing conditions: diagram depicting water-doping concentration and bite number by depth (A), diagram showing hole drilling locations accommodating 4 drill holes in regolith bin (B).

The regolith simulant bin used in this test was prepared using stratified moisture layers in which different weight percent (wt%) water-doped regolith simulants are layered one over the other, with a thin sheet of aluminum foil separating the layers to retain water content during atmospheric (unfrozen) conditions (Figure 4A). The regolith bin consisted of approximately 100 kg of water-doped lunar highlands simulant (NU-LHT-3M). The layers were vibrationally compacted in 20 cm increments to a density of approximately 1.6 g/cm^3. The water concentration increased with depth to simulate a stratification in water concentration versus drilled depth. The three moisture levels within the bin were "dry," 2.5 wt%, and 5 wt%. The dry moisture level was measured to contain approximately 0.2 wt% water due to adsorption from the atmosphere (Kleinhenz and Linne, 2013; Kleinhenz, 2014). These moisture levels were based on the expected water concentration as detected by LCROSS (Colaprete *et al.*, 2010). A brief description of all test conditions can be reviewed in Table 1.

Table 1: Summary of test conditions for drill sampling of regolith simulant as discussed above and shown in Figure 4.

Test Conditions	
Average Regolith Temperature	-178°C
Average Chamber Pressure	1.6 x 10^{-6} Torr
Bin Preparation	Top (0-24 cm): Dry Middle (24-48 cm): 2.5 wt% Bottom (48-117 cm): 5 wt%
Bite Depth	8 cm
Hole 1 Approach	All bites: 1 h hold
Hole 2 Approach	Bite 1: 5 min hold Bites 2-10: 10 min hold
Hole 3 Approach	Bite 1: 5 min hold Bites 4-6: 10 min hold Bites 7-10: 15 min hold
Hole 4 Approach	Bite 1: 5 min hold Bites 4-6: 10 min hold Bites 7-10: 15 min hold

2. Results and Discussion:

2.1. MSolo Responses to Drilling Operations

After each drill bite, all drill activities were paused while MSolo measured the evolution of volatiles from the pile. After the water signal (*m/z* 18) returned to baseline or a near-baseline value, the drill would then proceed to the next bite. While the focus of the test was to observe the water signal (*m/z* 18), other volatiles were also used to guide the MSolo team during drilling events. One notable example is the observed changes in the hydrogen signal (*m/z* 2), which was found to correlate with drilling. The hydrogen signal increased as the drill began to rotate, decayed as the drill retracted, and returned to baseline when the drill stopped. The hydrogen signal dynamics were unique from the evolved water signal dynamics, visible in Figure 5**Error! Reference source not found.**. It was later determined that the hydrogen signal activity was caused by the release of hydrogen from metal-on-metal interactions within the drill, as the hydrogen signal (*m/z* 2) only increased in activity when the drill was in motion.

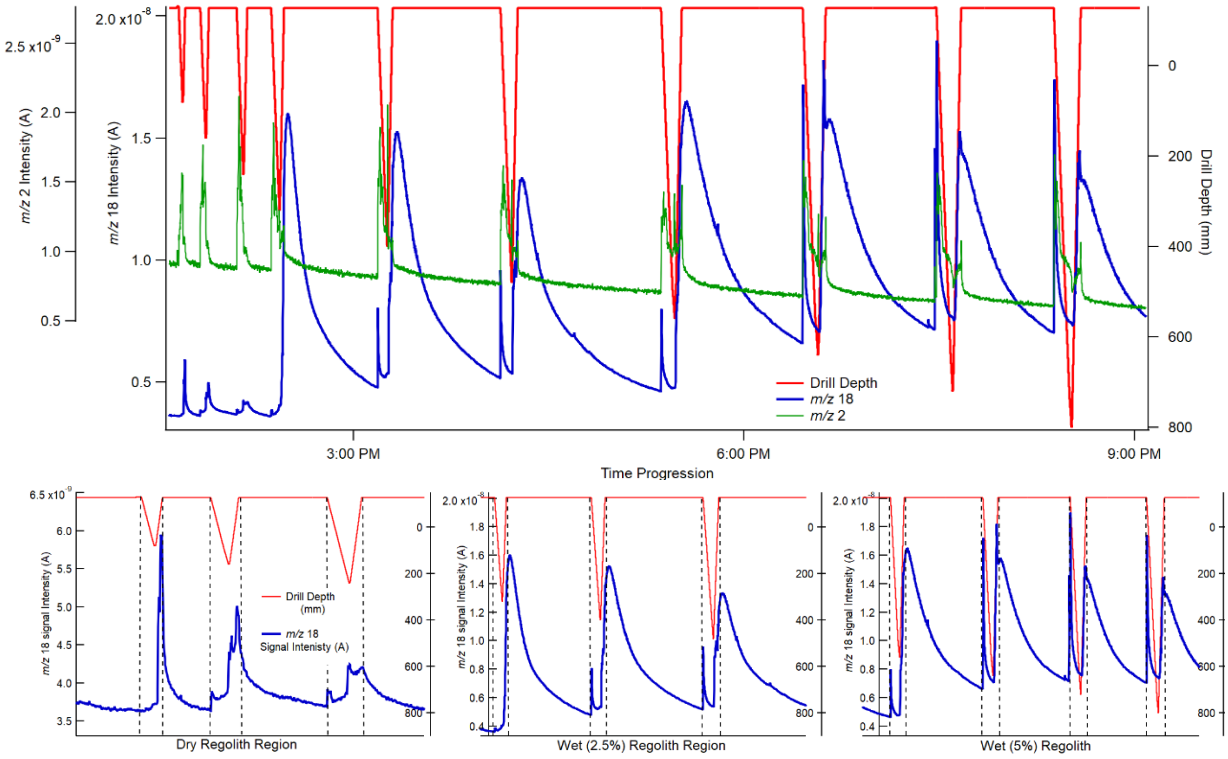

Figure 5: MSolo detection response during drill operations (top), zoomed sections for each region (bottom).

The signals measured by MSolo as a result of drilling the first hole are shown in Figure 5, where a spike in the water signal (*m/z* 18) was observed when regolith simulant material was extracted from the hole and deposited onto the surface, followed by a signal decay as the volatile activity reduced and therefore signal returns to a near-baseline value. This signal profile was even observed in the "dry" regolith region, demonstrating that the very low water concentration of 0.2 wt% could still be detected. There were also additional water signal spikes during drill movement activities, such as when the drill was lowered back into the drill hole or retracted out of the hole. This is visible for bites 2-10, but not for bite

1. These spikes in the water signal (*m/z* 18) likely come from the agitation of a previous drilling sample retained on the auger and/or from agitation of the cuttings pile. This theory is further supported by a similar water spike observed when the drill was lowered and retracted in a fashion so as to remove any remaining material from the drill brush. Figure 6 shows that even during dynamic environmental circumstances including changing chamber pressure and a dominant, progressively decreasing nitrogen signal (m/z 28), MSolo has the capacity to observe the evolution of lower-signal volatiles.

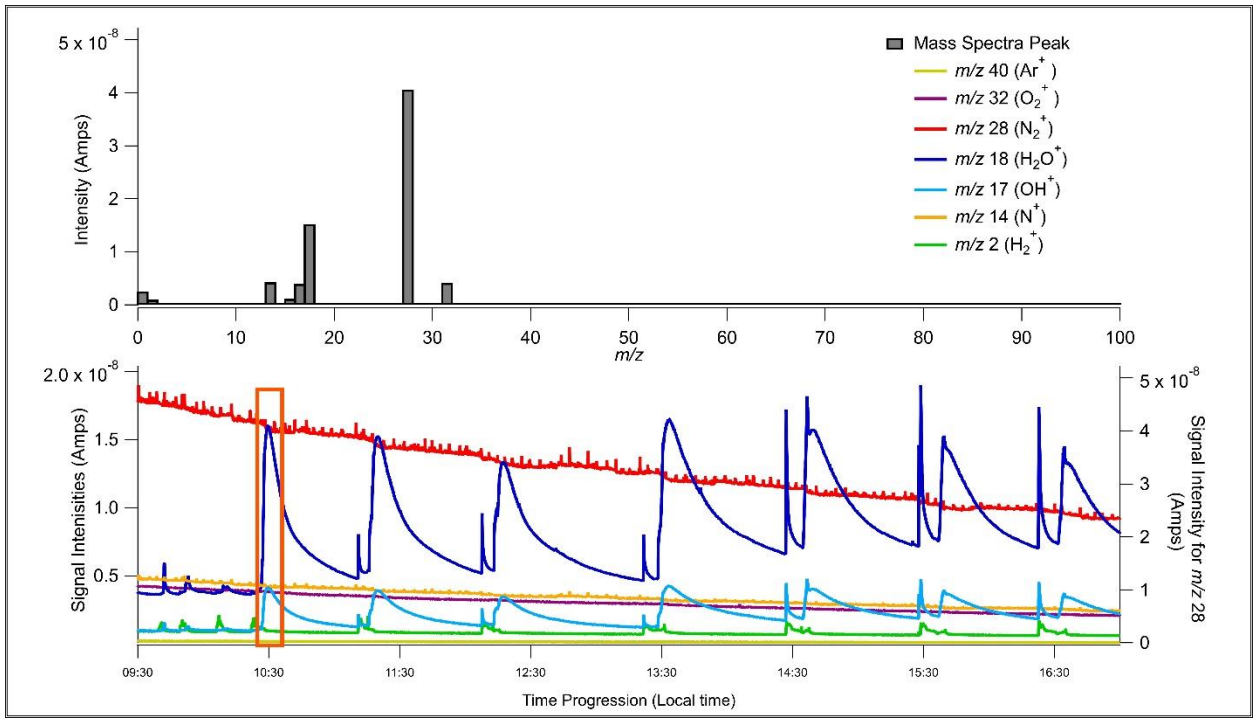

Figure 6: Individual mass spectra (top) during a peak signal (orange square) of water from drilling operations (mass trace - bottom).

The original plan for the test campaign was to permit the water signal to decay back to its baseline value prior to restarting drilling rotations, however, it was determined post-hole 1 that this would not be feasible, as the time it would take to return to baseline exceeded the total test duration. Table 1 describes that the drill position was maintained and drill activities paused for one hour between bites for hole 1, however, the pause was decreased to no more than 15 minutes for holes 2-4 in order to focus on capturing the shape of the initial evolution of the water peak observed during hole 1 drilling.

2.2. MSolo Measurements

As stated previously, three moisture levels were selected for the test: dry (< 0.2 wt%), 2.5 wt%, and 5 wt%. Figure 7 shows the evolution of the water signal (*m/z* 18) observed by MSolo throughout the drilling process. The water concentrations correlating with the drilling depth are depicted with different colored shading. Each bite is labeled on the graphs with the hole and bite number – HXBY – where X is the hole number and Y is the bite number. The label location is close to the estimated maximum result from each bite, and it should be noted that although some peaks are of higher intensities, these are due to secondary events such as regolith coming off the drill brush. Other events such as drill percussion and drill rotations are annotated for holes 1, 3, and 4, where a corresponding water signal increase was subsequently detected. Agitation of regolith material remaining within the drill, on the brush, and/or the regolith pile was determined to have caused these volatile releases. Furthermore, spikes in the water signal for all holes can be seen just prior to the secondary/decay spike, highlighted by a red square in Figure 7 for H1B5. This phenomenon is attributed to the release of residual regolith sample remaining on the drill bit upon drill rotation start up. While the deposit of this residual material resulted in the observe

sharp signal increases, the signal decayed quickly and did not disturb the signal trace from the new material brought to the surface during the subsequent bite's drilling operation.

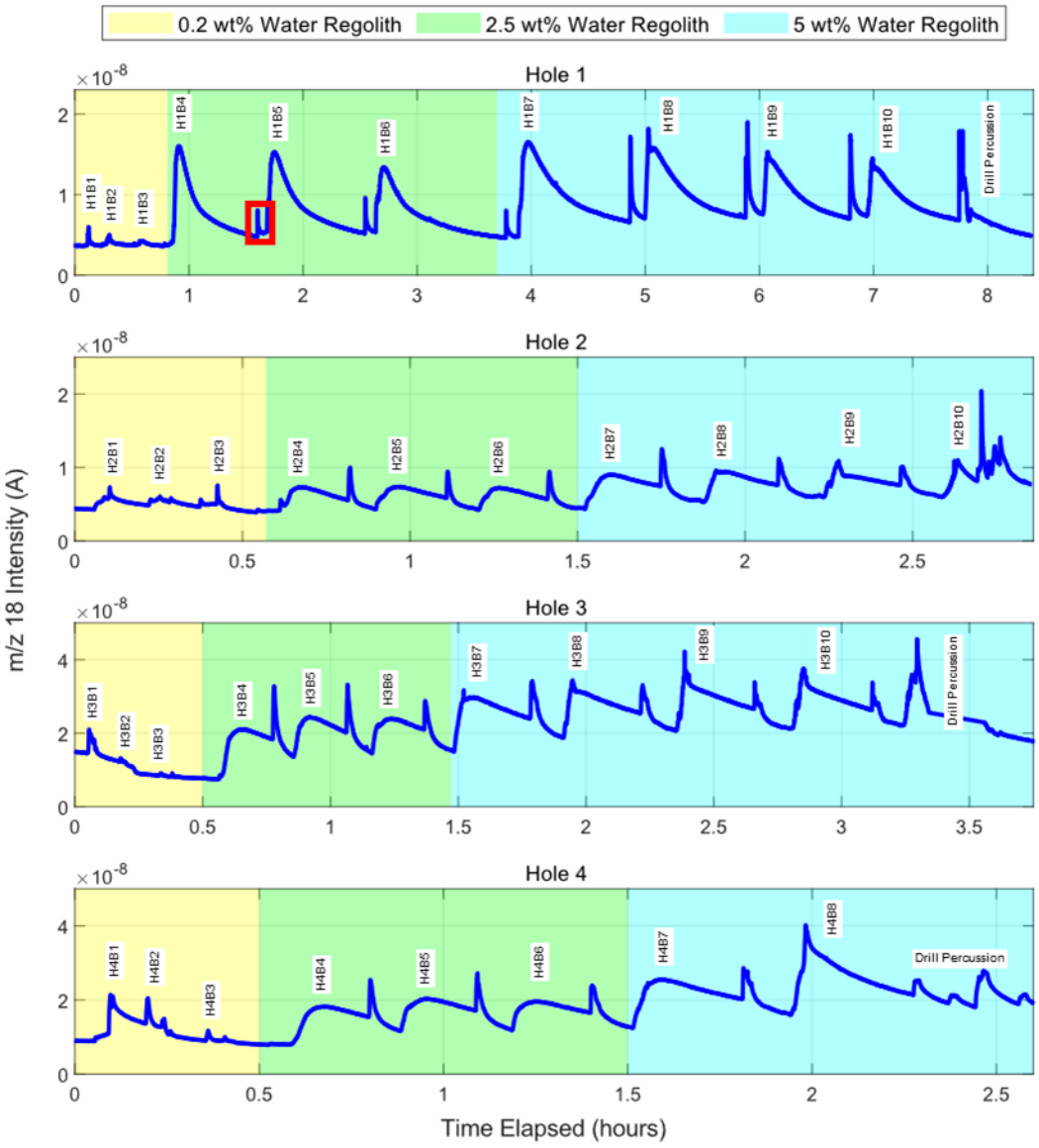

Figure 7: Evolution of water signal detected by MSolo throughout drilling operations.

Hole 1, bites 1-3 exhibit the lowest maximum signal intensities for the entire testing series. The max peak signal intensities for H1B1-H1B3 correspond to 5.95×10^{-9} A, 5.0×10^{-9} A, and 4.2×10^{-9} A respectively, and while low in intensity when compared to the rest of the evolved peaks, they are well above the baseline signal of the instrument (3.71×10^{-13} A) even while the pressure of the chamber is in

the low 10^{-6} Torr range. In contrast, H1B4-H1B10 show an increase in the water signal (*m/z* 18) during the drill activities, corresponding to the higher concentrations of water present in the regolith. There is also a distinctly higher water intensity for H1B7 than those of H1B8-H1B10, despite these bites all having the same water content. This signal response was attributed to the cuttings pile having reached the same height as the end of the drill chute and thus blocking the pile itself from uniformly distributing new material from the drill. The pile evolution is shown in Figure 8. The pile created by H1B7 would negatively affect the flow of extracted material by the remaining bites, and subsequently the signal intensities corresponding to those bites.

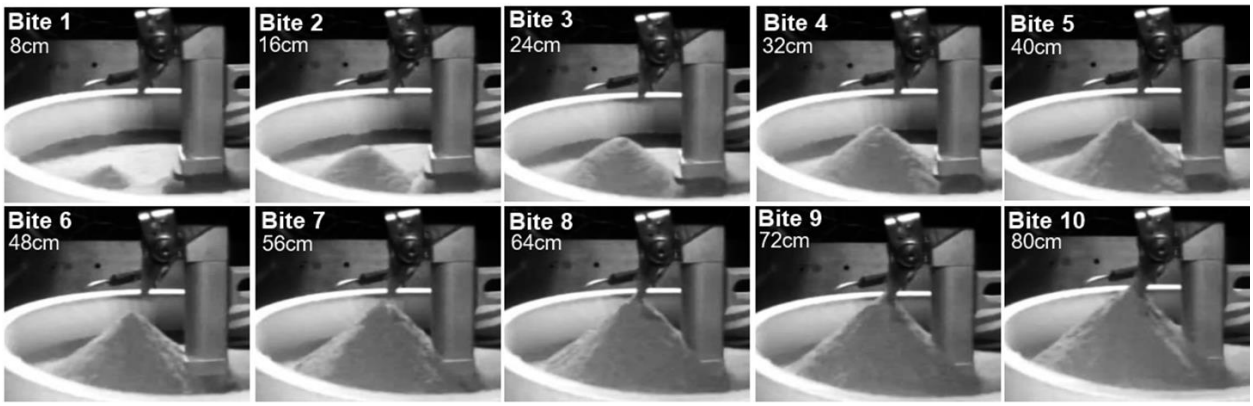

Figure 8: Video captures of cuttings pile progression for hole 1, each different bite and its resulting pile is shown.

Hole 2 water peak intensity values were overall lower that the rest of the drill holes, where H2B7 corresponding to the first bite in the 5% concentration resulted in a signal intensity of 8.9×10^{-9} A, compared to values of 1.65×10^{-8} A for H1B7, 2.94×10^{-8} A for H3B7, and 2.51×10^{-8} A for H4B7, respectively. This trend of lower signal intensities for hole 2 was attributed to a blockage of MSolo's FOV (calculated to be approximately 12%) by the multi-layer insulation (MLI) used to cover the trolley's gearbox system. In general, a negative signal intensity difference was observed when comparing intensity signals of each bite for hole 2 to hole 1.

For hole 3, bites H3B1 to H3B6 produced smooth water signal profiles as seen in Figure 7. However, from H3B7 to H3B10 a sharp spike-like signal was detected at the end of the drilling operations into the 5% doped regolith, most noticeably in H3B9 and H3B10. Closer inspection via the chamber-mounted cameras showed atypical regolith behavior correlating to the observed signal spikes. During the

later drilling activities of hole 3, sample pile disturbances were observed. Video showed that loose regolith surrounding the drill hole by the end of the drill chute began to fall back into the hole as the drill finished its retraction motion. It was this disruption of regolith that resulted in an unplanned release of volatile material during the drilling of this hole.

In the case of hole 4, a build-up of the pile cuttings similar to that of hole 1 resulted in an disproportionate flow of material coming off the drill chute. By the start of H4B8, a large overflow of cutting material began to fall from the edge of the regolith bin, causing a large water signal spike. Since any more material would only cause more disruptions, it was therefore determined that no more cuttings could be obtained for this hole, and the test was stopped after H4B8.

For the hole 1 bites, a stepwise increase in peak signal intensities per concentration depth was expected because the regolith was undisturbed prior to testing. Instead, a strong initial water signal spike occurred when drilling into a new concentration depth, followed by lower peak intensities despite the extracted material having the same concentration as the prior bites. Although there were some experimental setbacks during hole 2 operations, the same pattern for signal intensities can be seen from bite to bite, as was observed in hole 1. Holes 3 and 4 did not exhibit decreasing peak intensities within the same concentration of water in the regolith for bites 4-10 and 4-8, respectively, but did for the first three bites. Ignoring spikes attributed to avalanching regolith, for H3B4-10, the signals maintained consistent peak intensities within the same concentration layer. For H4B4-6, the signals were also consistent.

It is worth noting that the signals observed during the drilling of hole 1 are unaffected by potential contributions from regolith from previous holes, whereas signals for subsequent holes 2-4 may have been impacted. After hole 1, the drill was fully retracted, followed by a drill percussion to remove material from the drill. The pile was then flattened by the drill footpad to get the sampling surface as even as possible to prepare for the next drill hole. These activities caused the extracted material from deeper layers to be exposed and spread over the top (dry) layers, changing the initial conditions for the bites of the remaining holes. Though this surface contamination appeared to affect the signals associated with lower water concentration by creating a progressive elevated water baseline value visible in the yellow regions of Figure 7, it does not appear to have significantly disrupted the higher concentrations.

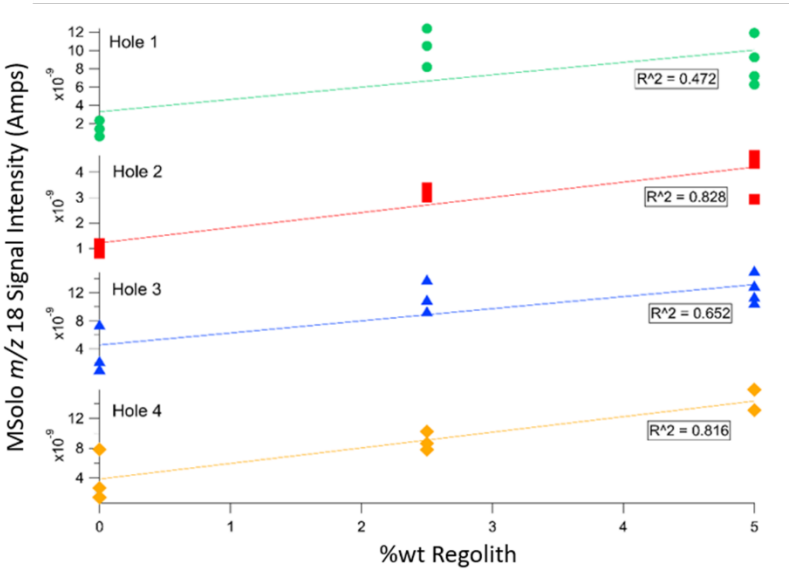

Figure 9: MSolo peak raw intensity correlation to wt% values.

Figure 9 shows the statistical correlation between the signal intensities detected for the water signal (*m/z* 18) and the corresponding wt% of the water in the simulant. Despite the effects of pile dynamics mentioned previously, an increase of signal intensity as a function of depth could be determined. hole 1 however, displayed a greater average peak signal for the 2.5 wt% water bites than the 5 wt% water bites, which is counter to what was expected.

3. Empirical Correlation

A quantitative relationship between the signals observed by MSolo during the test and the "visible" geometry of the regolith piles was assessed. This relationship provides a foundation for correlating the physical behavior of the water molecules as they evolve from the drill piles with the signals observed by MSolo. This relationship can be considered a pseudo-calibration curve with the potential to be used in real time during lunar missions, however, with notable limitations, to be discussed later.

An explanation for the decreasing signal pattern observed for bites within the same concentration layer in the first hole took into consideration the surface area of the pile. It is assumed that the same number of water molecules are contained within each bite for a particular concentration layer, and only the molecules in the most recent bite can travel to the instrument. It is known that the surface area of the pile increases with each bite. Therefore, the water molecules are less dense for repeated bites within a

layer of regolith at the same concentration. The signal observed by MSolo is dependent on the number of molecules capable of reaching the detection zone of the instrument. With a constant instrument position, and with each bite decreasing the density of water molecules, fewer molecules can enter the instrument, and thus signal decreases for each bite within the same concentration.

Utilizing cameras located adjacent to and above the bin, the diameter and height of the cuttings pile from each bite was measured and used to calculate the conical surface area of the pile. The pile size increases with each bite, and as such, the conical surface area increases with each bite. The initial water concentration at each depth was known (< 0.2 wt%, 2.5 wt%, and 5.0 wt% water) as was the volume of each bite, thus, the total amount of water in each bite could be approximated. Assuming that water could only sublimate from the newest bite volume, the water sublimation fluence is the approximated total amount of water per bite divided by the surface area of the pile. It is assumed that this water fluence is representative of the flux of molecules that are detected by MSolo. It is important to note that the projected aperture area onto the pile surface is not explicitly accounted for during this approximation. Bites 1-3, 4-6, and 7-10 each had the same concentration of water and thus the same number of water molecules, respectively, but their total conical surface areas increase as the pile size increased. Therefore, there is a decrease in water density and decrease in fluence following the initial bite at the new concentration, similar to the decrease in the water signal (*m/z* 18) intensity from MSolo (Figure 10**Error! Reference source not found.**). This phenomenon was evident in holes 1, 2, and 3. However, the pile falling over the edge of the bin in hole 4 bite 8 resulted in a water intensity that was greater than what was expected. Figure 10 overlays the peak signals observed for each bite for each hole (line plot) with the water fluences calculated from the dimensions of the piles generated from the drilling of hole 1 (bar chart), as only measurements of pile radius and height for hole 1 were available.

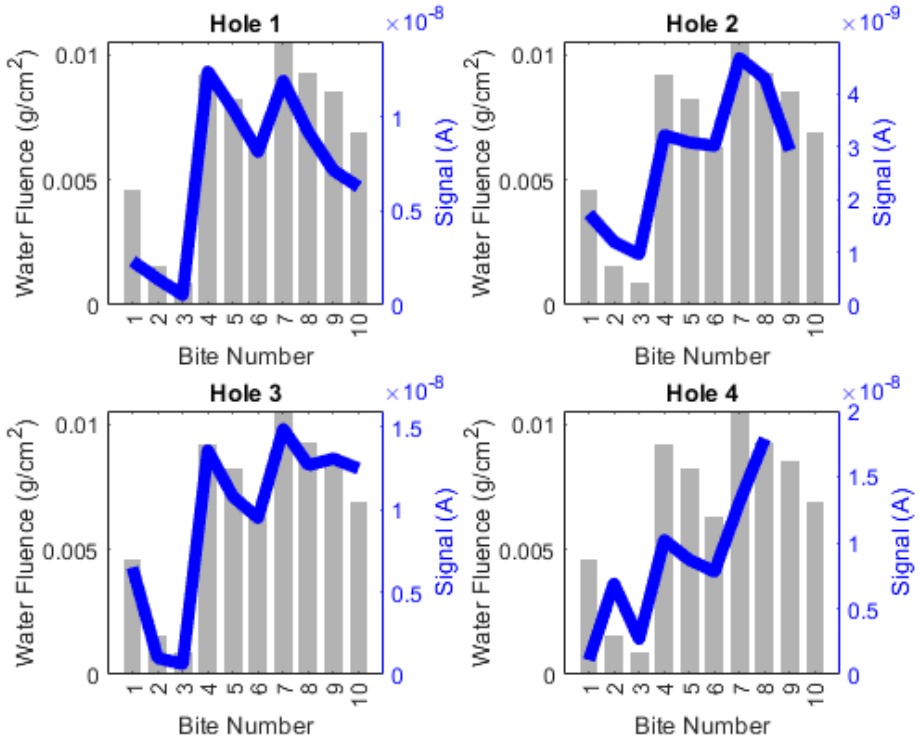

361

362 Figure 10: Water fluence per cm^2 (bar graph) and the water signal (*m/z* 18) intensity (line graph) for holes
363 1-4.

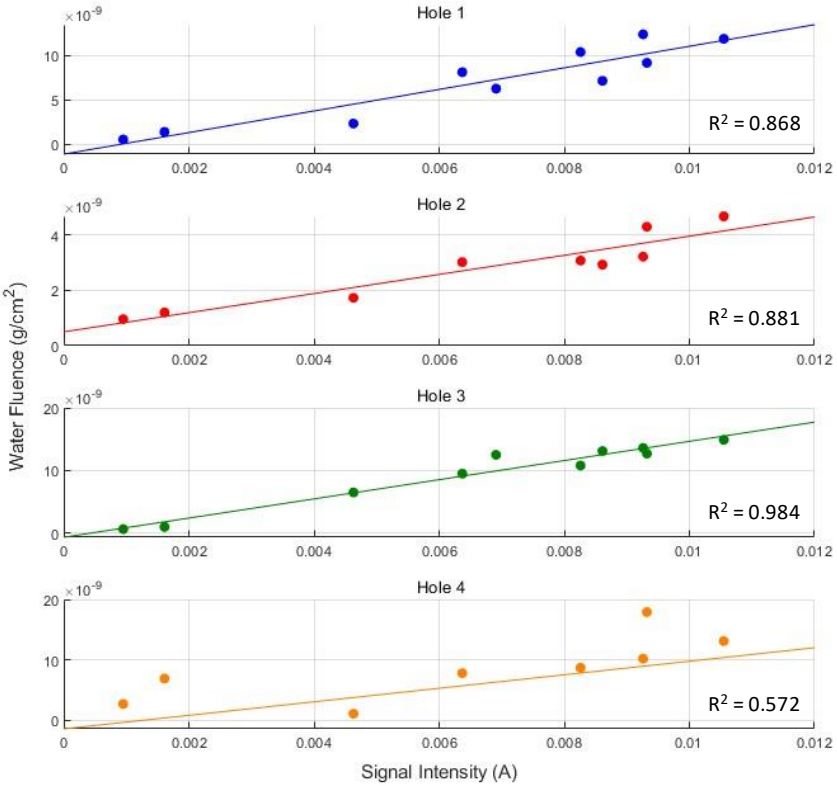

Figure 11: Water fluence per cm^2 versus *m/z* 18 intensity shows a linear relationship between the two parameters. The solid line is the linear best-fit line.

The relationship between the water fluence and the water signal (*m/z* 18) was plotted for each hole and shown to have a roughly linear relationship (see Figure 11). This water fluence is not a measured quantity, but an approximation based on the volume of the bite and the approximate density of packed regolith (Connolly and Carrier, 2023), and this value is divided by the conical surface area calculated from pile measurements. As only hole 1 pile dimensions were measured, these dimensions were used for the water fluence for holes 3 and 4, as well. The R-squared values for holes 1-3 were all above 0.85, with hole 3 reporting 0.98.

This linear relationship between the water fluence and observed signal was used to generate a MATLAB code that takes in inputs of measured pile radius, height, bite depth, partial pressure of water (a value derived from the measured signal, the instrument sensitivity, the instrument gain, and several other constants) and outputs an approximation for the wt% of water in the regolith. To compare the

signals from the different depths and drill holes, it is assumed that the drill cuttings are deposited from the drill at the same temperature for each bite.

The water fluence per bite was fit to the peak signal intensities measured for holes 1, 3 and 4 as shown in the plot below. Hole 2 was not included because MSolo's FOV was blocked during drilling of this hole as mentioned previously.

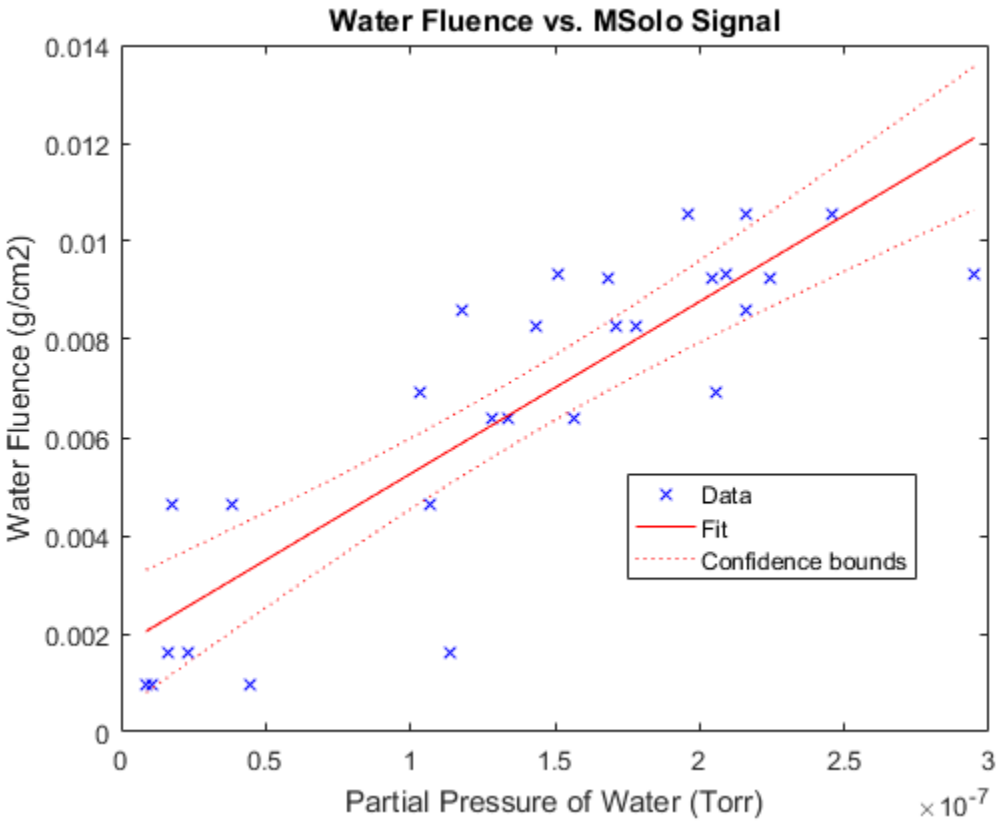

Figure 12: Linear regression fitting an approximation for water fluence from the regolith piles to the partial pressures of water observed during GRC testing.

The algorithm used with this fit within the MATLAB code is as follows:

1. The total mass per bite is calculated by approximating the bite volume as a cylinder using the radius of the drill and the depth of the bite as the height. This volume is then multiplied by the density of packed regolith determined during the regolith preparation.

2. The surface area of the pile is calculated from the measured radius and height of the pile.
3. The measured peak signal from the MSolo instrument is converted to a partial pressure using the instrument gain and sensitivity, in addition to other constants.
4. The fit is used to convert the partial pressure to the water fluence.
5. This water fluence is multiplied by the surface area calculated in step 2 and divided by the total bite mass calculated in Step 1 to produce the wt% per bite.

The MSolo signals, pile heights and radii from hole 1 were used as inputs to this algorithm and generated the plot in Figure 13. The output wt% values fall within a 95% prediction interval of the predicted wt%. A prediction interval was used in this analysis as the goal is to predict the result of a single future observation rather than an average of several observations (Faraway, 2009). The prediction intervals increase with the bite number as the prediction interval is calculated from the water fluence vs. partial pressure relationship and then converted from representing water fluence to representing mass fraction using the conversion explained above in step 5. The conversion value increases with bite number because the surface area of the pile increases with additional bites while the total mass of the bite stays approximately the same, causing the calculated prediction interval to increase as well (see "Supplementary Section" for explicit calculations).

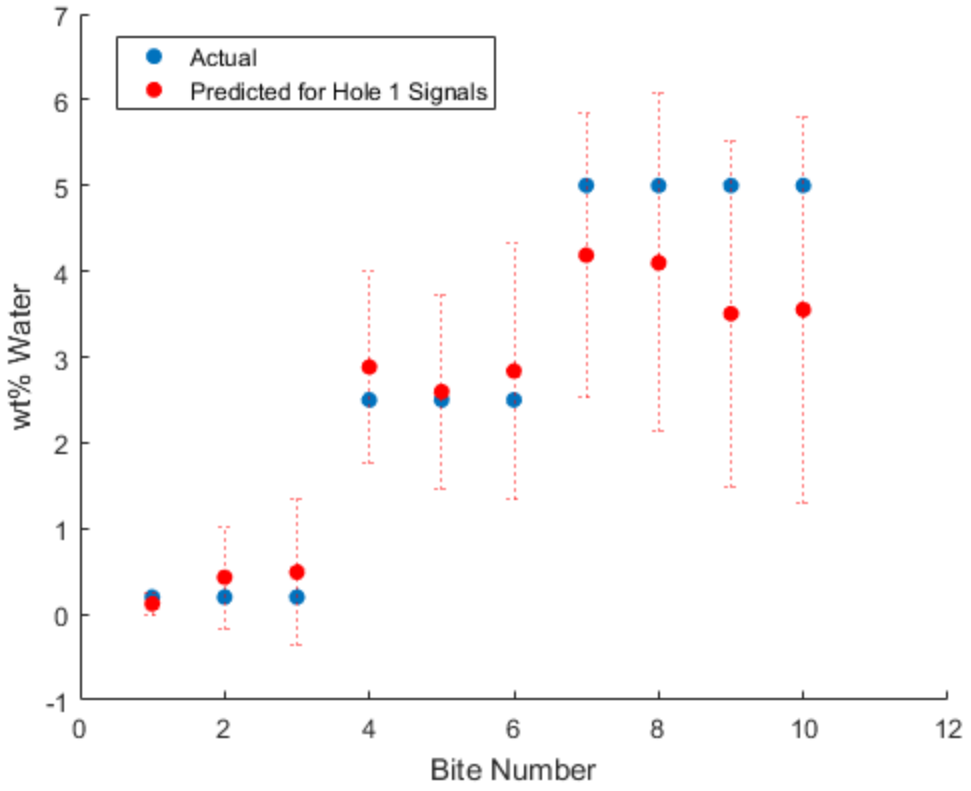

411

412 Figure 13: Predictions for the wt% water for each bite generated from hole 1 signal inputs and the
413 MATLAB algorithm

414

415 MSolo detects gases whose behavior is dependent on temperature, therefore, a scale factor to
416 adjust the signal-wt% relationship will likely be necessary in order to effectively use the empirical
417 correlation, as the lunar surface will have different environmental conditions than in the test case. An
418 initial scale factor based on the equation for sublimation per surface area (Andreas, 2007) was
419 calculated. The scale factor is a ratio of the sublimation per surface area at the GRC conditions over the
420 sublimation per surface area at an input temperature condition. Based on the temperature dependence
421 of this equation, it can be estimated that the water fluence from the piles in permanently shadowed
422 lunar crater conditions (50 K plus 60 K added for regolith heating by the drill) would be 25 million times
423 less than the fluence measured during the terrestrial test (100 K plus 60 K). As such, we took an average
424 of the signals from the three holes for each bite and scaled these average signals down by an arbitrary
425 $1x10^{-8}$ to get reasonable wt% values. These signals were put into the MATLAB code along with an
426 assumed lunar surface plus heated regolith temperature of 110 K. Results are shown in Figure 14.

427

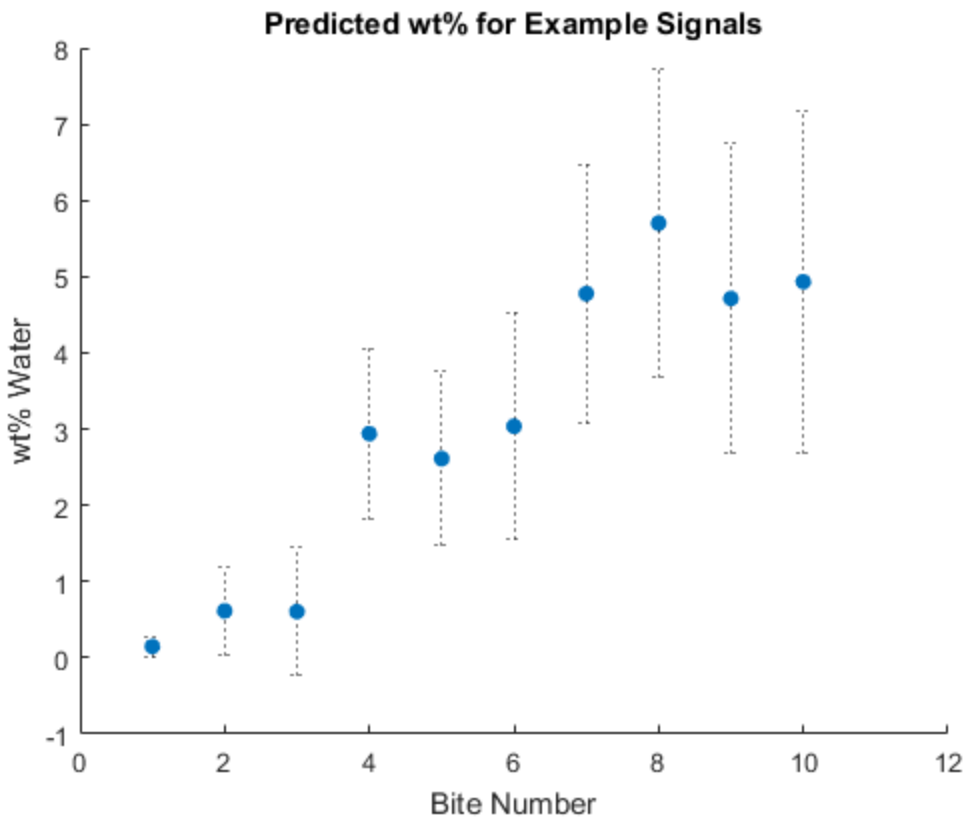

Figure 14: Predictions for the wt% water for each bite generated from sample signal inputs, lunar temperature, and the MATLAB algorithm.

It is obvious that this relationship is also imperfect. Scaling the average signals by $1x10^{-8}$ results in signals on the order of $1x10^{-17}$, which are below the limit of detection of MSolo. However, signals of this magnitude are necessary for the temperature scale factor at 110 K and the code to generate reasonable wt%, as shown in Figure 14. Typically, a calibration curve is only valid under the conditions in which it was developed because the behavior of instrument and the volatilized water could be affected by temperature and pressure. Though the GRC tests approached lunar surface conditions, there is divergence. The temperature scale factor was included to compensate for this, but it is not sufficient to account for other differences including pressure and physical characteristics of the regolith. The data used to generate the calibration curve was also highly variable and resulted in a curve fit with an R^2 value of only 0.75. Gathering additional data in the future will improve the robustness of this calibration curve in addition to making progress with understanding the phenomena observed during the GRC tests and thus, future development of theoretical models.

4. Conclusion

Despite the limitations of this test campaign, performing relative water quantifications based on MSolo's observed signal intensity during lunar drilling operations is possible. Relative quantification of the data is already possible via inspection of the raw data from the test—drilling regolith with the lowest concentration of water corresponded to the lowest signal obtained by MSolo, and drilling regolith with the highest concentration of water corresponded to the highest signals observed by MSolo. The empirical correlation shows promise as a starting point towards estimating absolute regolith water concentrations from MSolo signals, however, additional data is necessary to provide accurate and repeatable results.

Acknowledgements:

The authors would like to extend their gratitude to the entire PRIME-1 team and to the many contributions from members of the KSC Prototype Design Laboratory, the KSC Vibration Laboratory, and all other members who worked in the development of the MSolo and TRIDENT instruments. We would also like to thank the INFICON personnel for their assistance during the test campaign. We recognize NASA's Science Technology Mission Directorate (STMD) for their financial support of the testing campaign.

References

Andreas, E.L. (2007) 'New estimates for the sublimation rate for ice on the Moon', *Icarus*, 186(1), pp. 24–30. Available at: https://doi.org/10.1016/j.icarus.2006.08.024.

Colaprete, A. *et al.* (2010) 'Detection of Water in the LCROSS Ejecta Plume', *Science*, 330(6003), pp. 463–468. Available at: https://doi.org/10.1126/science.1186986.

Connolly, J. and Carrier, W.D. (2023) 'An Engineering Guide to Lunar Geotechnical Properties', in *2023 IEEE Aerospace Conference*. *2023 IEEE Aerospace Conference*, Big Sky, MT, USA: IEEE, pp. 1–9. Available at: https://doi.org/10.1109/AERO55745.2023.10115961.

Cui, J. *et al.* (2023) 'Simulation of Drilling Temperature Rise in Frozen Soil of Lunar Polar Region Based on Discrete Element Theory', *Aerospace*, 10(4), p. 368. Available at: https://doi.org/10.3390/aerospace10040368.

Faraway, J.J. (2009) *Linear models with R.* London: Chapman & Hall/CRC.

Feldman, W.C. *et al.* (1998) 'Fluxes of Fast and Epithermal Neutrons from Lunar Prospector: Evidence for Water Ice at the Lunar Poles', *Science*, 281(5382), pp. 1496–1500. Available at: https://doi.org/10.1126/science.281.5382.1496.

Fraser, H.J. *et al.* (2001) 'Thermal desorption of water ice in the interstellar medium', *Monthly Notices of the Royal Astronomical Society*, 327(4), pp. 1165–1172. Available at: https://doi.org/10.1046/j.1365-8711.2001.04835.x.

Kleinhenz, J. and Linne, D. (2013) 'Preparation of a Frozen Regolith Simulant Bed for ISRU Component Testing in a Vacuum Chamber', in *51st AIAA Aerospace Sciences Meeting including the New Horizons Forum and Aerospace Exposition*. *51st AIAA Aerospace Sciences Meeting including the New Horizons Forum and Aerospace Exposition*, Grapevine (Dallas/Ft. Worth Region), Texas: American Institute of Aeronautics and Astronautics. Available at: https://doi.org/10.2514/6.2013-732.

Kleinhenz, J.E. (2014) 'Lunar Polar Environmental Testing: Regolith Simulant Conditioning', in *7th Symposium on Space Resource Utilization*. *7th Symposium on Space Resource Utilization*, National Harbor, Maryland: American Institute of Aeronautics and Astronautics. Available at: https://doi.org/10.2514/6.2014-0689.

Li, Y. *et al.* (2023) 'The Mechanism for the Barrier of Lunar Regolith on the Migration of Water Molecules', *Journal of Geophysical Research: Planets*, 128(3), p. e2022JE007254. Available at: https://doi.org/10.1029/2022JE007254.

Metzger, P.T., Zacny, K. and Morrison, P. (2020) 'Thermal Extraction of Volatiles from Lunar and Asteroid Regolith in Axisymmetric Crank–Nicolson Modeling', *Journal of Aerospace Engineering*, 33(6), p. 04020075. Available at: https://doi.org/10.1061/(ASCE)AS.1943-5525.0001165.

Metzger, P.T., Zacny, K. and Morrison, P. (2021) 'Erratum for "Thermal Extraction of Volatiles from Lunar and Asteroid Regolith in Axisymmetric Crank-Nicholson Modeling" by Philip T. Metzger, Kris Zacny, and Phillip Morrison', *Journal of Aerospace Engineering*, 34(5), p. 08221002. Available at: https://doi.org/10.1061/(ASCE)AS.1943-5525.0001312.

Murphy, D.M. and Koop, T. (2005) 'Review of the vapour pressures of ice and supercooled water for atmospheric applications', *Quarterly Journal of the Royal Meteorological Society*, 131(608), pp. 1539–1565. Available at: https://doi.org/10.1256/qj.04.94.

Nozette, S. *et al.* (1996) 'The Clementine Bistatic Radar Experiment', *Science*, 274(5292), pp. 1495–1498. Available at: https://doi.org/10.1126/science.274.5292.1495.

Paulsen, G. *et al.* (2018) 'The Regolith and Ice Drill for Exploration of New Terrains (TRIDENT); a One-Meter Drill for the Lunar Resource Prospector Mission'. Available at: https://esmats.eu/amspapers/pastpapers/pdfs/2018/paulsen.pdf.

Roozbahani, M., Borela, R. and Frost, J. (2017) 'Pore Size Distribution in Granular Material Microstructure', *Materials*, 10(11), p. 1237. Available at: https://doi.org/10.3390/ma10111237.

Sanders, G.B. and Larson, W.E. (2013) 'Progress Made in Lunar In Situ Resource Utilization under NASA's Exploration Technology and Development Program', *Journal of Aerospace Engineering*, 26(1), pp. 5–17. Available at: https://doi.org/10.1061/(ASCE)AS.1943-5525.0000208.

Simon, L. *et al.* (no date) *STAT 501: Regression Methods*, *Penn State Eberly College of Science*. Available at: https://online.stat.psu.edu/stat501/ (Accessed: 24 April 2025).

Wilkerson, R.P. *et al.* (2023) 'Outgassing behavior and heat treatment optimization of JSC-1A Lunar regolith simulant', *Icarus*, 400, p. 115577. Available at: https://doi.org/10.1016/j.icarus.2023.115577.

Zacny, K. *et al.* (2023) 'TRIDENT Drill for VIPER and PRIME-1 Missions to the Moon', in *Earth and Space 2022*. *18th Biennial International Conference on Engineering, Science, Construction, and Operations in Challenging Environments*, Denver, Colorado: American Society of Civil Engineers, pp. 465–474. Available at: https://doi.org/10.1061/9780784484470.043.

Supplementary Section

Confidence Interval Calculation

The Linear Regression fit of the "water fluence" (y data) to the partial pressure of water (x data) is used to calculate a 95% prediction interval using the equation for standard error of the prediction:

$$PI = \hat{Y}_h \pm t \times \sqrt{MSE \times \left(1 + \frac{1}{n} + \frac{(X_h - \bar{X})^2}{\sum(X_i - \bar{X})^2}\right)}$$

Where PI is the 95% confidence interval, $\hat{Y}_h$ is the predicted value generated from a predictor value, X_h, t is the t-value which depends on the confidence level and degrees of freedom n, MSE is the mean square error calculated using the equation below, $\bar{X}$ is the mean of the known x-data used to determine the fit, and X_i is the ith known x value (one of the dataset used to calculate the fit)(Simon *et al.*, no date).

The mean square error is computed as follows:

$$MSE = \frac{1}{n}\sum_{i=1}^{n}(Y_i - \hat{Y}_i)^2$$

Where Y_i is the known y-data, $\hat{Y}_i$ is the y-data generated from the known x-data by the fit, and n is the total number of points of known data.

t for the 95% confidence interval is computed using MATLAB's built-in tinv function.

$\hat{Y}_h$ is calculated using the linear fit.

PI can then be calculated according to the equation above.

To convert PI to a representation of our quantity of interest – the mass percent water – PI is then multiplied by the surface area of the pile at a particular bite over the total mass per bite.

The error bars in Figure 17 are the result of multiplying the second term in the PI equation by the surface area of the pile at a particular bite over the total mass per bite, as mentioned in previous sections. The surface area of the pile increases with the number of bites, while the total mass per bite stays the same, resulting in a larger interval with larger bites.